



1 **On the use of Weather Regimes to forecast meteorological drought over**

2 **Europe**

3 Christophe Lavaysse*

4 *European Commission, Joint Research Centre (JRC), 21027 Ispra (VA), Italy*

5 *Univ. Grenoble Alpes, CNRS, IRD, G-INP, IGE, F-38000 Grenoble, France*

6 Jürgen Vogt, Andrea Toreti

7 *European Commission, Joint Research Centre (JRC), 21027 Ispra (VA), Italy*

8 Marco L. Carrera

9 *Environment and Climate Change Canada, Dorval, QC, Canada*

10 Florian Pappenberger

11 *ECMWF, Reading, United Kingdom*

12 *Corresponding author address: European Commission, Joint Research Centre (JRC), 21027 Ispra
13 (VA), Italy

14 E-mail: christophe.lavaysse@ird.fr



ABSTRACT

15 An early warning system for drought events can provide valuable informa-
16 tion for decision makers dealing with water resources management and inter-
17 national aid. However, predicting such extreme events is still a big challenge.
18 In this study, we compare two approaches for drought predictions based, re-
19 spectively, on forecasted precipitation derived from the extended ENSEMBLE
20 system of the ECMWF, and on forecasted Monthly Occurrence Anomaly of
21 Weather Regimes (MOAWRs) also derived from the ECMWF model.
22 Results show that the MOAWRs approach outperforms the one based on fore-
23 casted precipitation in winter in the northern and eastern parts of the European
24 continent, where more than 65% of droughts are detected one month in ad-
25 vance. While, the approach based on forecasted precipitation achieves better
26 performance in predicting drought events in central and eastern Europe in
27 both spring and summer, when the local atmospheric forcing could be the key
28 driver of the precipitation. Sensitivity tests also reveal the challenges in pre-
29 dicting small-scales and onset drought events at longer lead times.
30 Finally, in most of the cases, the ENSEMBLE system of the ECMWF success-
31 fully represents the observed large scale atmospheric patterns, depicted by the
32 MOAWRs, associated with drought events over Europe.



33 **1. Introduction**

34 Developing a robust early warning system for drought events is a key challenge for modelers
35 and forecasters. The timescale of these events (generally from one to several months) requires
36 accurate forecasts with long lead times. Due to the uncertainties of the models, the chaotic nature
37 of the atmospheric circulation and the errors in the initial conditions, the reliability of precipitation
38 forecasts is close to climatology beyond a 9-day lead time (Haiden et al. 2017). In a recent study
39 (Lavaysse et al. 2015), it has been shown that about 40% of the meteorological droughts, defined
40 by an anomaly of the standardized precipitation index (SPI), can be detected one month in advance
41 by using the forecasted precipitation provided by the ECMWF extended ensemble. These forecasts
42 might be improved by using post-processing techniques or predictors that are better simulated by
43 atmospheric models. Most of the large-scale variability of rainfall and drought events is generated
44 by specific large-scale circulation patterns.

45 The concept of Weather Regimes (WRs) was first introduced in the early 1950s, on the assump-
46 tion that the atmosphere evolves between a finite number of large-scale circulation states. It is
47 based on recurrent, persistent and/or quasi stationary states of the atmosphere (Michelangeli et al.
48 1995; Stephenson et al. 2004). They are well known to play an important role in creating large-
49 scale conditions that either favor or inhibit precipitation in Europe, especially extreme events (Boé
50 2013; Guérémy et al. 2012; Yiou and Cattiaux 2013; Cattiaux et al. 2010; Toreti et al. 2010). These
51 impacts can be observed in both winter and summer, and for different meteorological fields such
52 as wind gusts and temperature extremes (Pfahl 2014). In Europe, WRs are highly teleconnected to
53 temperature anomalies at the surface and precipitation (Plaut and Simonnet 2001; Yiou and Nogaj
54 2004) and well identifiable spatial patterns of these two variables are associated with each regime.
55 For instance, the positive North Atlantic Oscillation phases (NAO+) in winter are teleconnected



56 to above-normal temperature and precipitation over Northern Europe and below-normal precipita-
57 tion over Southern and Central Europe (Wanner et al. 2001; Hurrell et al. 2003). Opposite results
58 of surface temperature and precipitation anomalies are generally observed during negative NAO
59 phases (NAO-). The WRs also have an impact on extreme events. The NAO+ regime favors heavy
60 precipitation in northern Europe and periods of drought in the Mediterranean area. The Blocking
61 regime determines the occurrence of dry periods in large parts of southern Scandinavia and central
62 Europe (Yiou and Nogaj 2004). The use of WRs is also interesting since their occurrence and
63 variability are connected to SST anomalies (Zampieri et al. 2017; Peings and Magnusdottir 2014;
64 Häkkinen et al. 2011) and thus somehow takes implicitly into account the Atlantic ocean influence.
65 The practical interest in classifying large-scale geopotential anomalies into a few pre-defined pat-
66 terns relies on the fact that local weather conditions depend on large-scale atmospheric flows. If
67 WRs can be better represented and forecasted by general circulation models (GCMs), they would
68 provide additional information for local weather anomalies via statistical downscaling techniques,
69 which derives teleconnections in between large scale geopotential anomalies (e.g., the WRs) and
70 local weather phenomena (e.g., precipitation anomalies). Since geopotential and temperature
71 fields are generally better forecasted than precipitation in Numerical Weather Prediction systems
72 (Vitart 2014), we here analyze the benefit of using WR occurrences as predictor of drought occur-
73 rence. A recent study carried out on the large scale forcing of long-term droughts has highlighted
74 its potential interest for Europe (Kingston et al. 2015).

75 Therefore, the objective of this study is to analyze the potential benefit of using atmospheric pre-
76 dictors, and more specifically the WR occurrences, to forecast meteorological droughts in Europe.
77 The paper is organized into six sections. The datasets and the methods are presented in section 2,
78 the different forecast methods in section 3. The comparison of predictability scores obtained by



79 using precipitation and MOAWRs is provided in section 4. The sources of uncertainties are then
80 discussed in section 5 and the main conclusions are drawn in section 6.

81 **2. Data and methods**

82 *a. Datasets*

83 The observed daily cumulated precipitation data are retrieved from the Climate Assessment &
84 Dataset (ECA&D) and the ENSEMBLES gridded dataset (E-OBS) version 12, which provides ob-
85 servational daily station-based precipitation and temperature data on regular grids (Haylock et al.
86 2008). While the full E-OBS resolution is 0.25 degrees, data have been here upscaled by averag-
87 ing to 1 degree due to the specific focus on large-scale drought with significant socio-economic
88 impacts. E-OBS data are available from 1950 to the present.

89 Atmospheric predictors are identified by using the geopotential height at 500 hPa. The daily
90 geopotential is derived from the ERA Interim reanalysis (ERA-Interim, Dee et al. 2011) with a spatial
91 resolution of 1.125 degrees covering the period from 1979 to the present.

92 The observed precipitation and the WR-based forecasts are compared to the forecast of precip-
93 itation taken from the extended ensemble system of the ECMWF (ENS hereafter, Molteni et al.
94 1996). The ENS is the latest version of the ECMWF ensemble model. In 2012, it was extended
95 once a week to a 32-day lead time and the horizontal resolution varies from T1639 (32 km) from
96 t+0 to t+10days to T1319 (64 km) from t+11 to t+32days. All of these datasets have been re-
97 gridded onto a regular grid of 1-degree resolution based on an averaging up-scaling method. The
98 rationale of using coarser resolution is i) to detect and so focus on larger scale precipitation deficits
99 and ii) to take into account spatial bias in the model that could detect the right precipitation signal
100 but with a slight spatial phasing error. The ENS is composed of one unperturbed member and



101 50 perturbed members, distinguished by different initial conditions and representations of model
102 uncertainties. In addition to these forecasts, the ECMWF produces hindcasts that are launched the
103 same date of the ENS for the last 20 years with five members only. To compute the forecasted
104 WRs, the daily geopotential fields at 500 hPa for each member are extracted from the ENS system
105 in both the hindcast and the forecast periods.

106 In order to build the baseline (following a normalization technique) and to have a time series
107 long enough to calculate the scores, 21 years of hindcasts (November 1992 to November 2013)
108 and the forecasts (November 2012 to November 2014) are used. To be coherent, the datasets of
109 observed precipitation and the WR calculations (from ERAI) are restricted to the same period.

110 *b. Weather regimes*

111 The WR classification (i.e. definition of the WR patterns) is done, exclusively using ERAI, by a
112 K-means method nested within a genetic algorithm to avoid dependence on the initial conditions
113 and the trap of the local minima (Toreti et al. 2010). The four meteorological seasons are treated
114 independently: winter (December to February), spring (March to May), summer (June to August)
115 and autumn (September to November) but to avoid inconsistency moving from one season to an-
116 other, each season is extended by adding the last month of the previous season. This method of
117 classification has been extensively used (Michelangeli et al. 1995; Santos et al. 2005; Robertson
118 and Ghil 1999), but because in this study the WR classification needs to fit with specific requests
119 (20-year moving period of the hindcast, the four seasons), it is important to regenerate this classifi-
120 cation. Nevertheless, the patterns of the geopotential anomalies (shown in Fig. 2 in supp. material
121) are strongly similar to those obtained in previous studies mentioned earlier. The choice of using
122 only the ERAI classification and not ENS is justified by: i) looking at previous studies that have
123 shown the relatively similar behavior of ERAI and ENS forecasts (Ferranti et al. 2015); ii) consid-



124 ering that this choice avoids inconsistency (or the impossibility to derive a coherent classification)
125 due to the continuous evolution of the ENS model. Four WRs are identified in winter and spring,
126 while three WRs are detected in summer and autumn (see Fig. 2 in the supplementary material).
127 The number of WRs is estimated by following Toreti et al. (2010) and depends both on the period
128 (here from 1992 to 2013) and the region (North Atlantic) studied. This is why the number of
129 summer WRs is different with respect to, e.g., Cassou et al. (2005).

130 Then, an assignation procedure is run to identify The closest WR to a given daily geopotential
131 anomaly of ERAI and a given ENS-member. To this aim, the method proposed by Ferranti et al.
132 (2015) is here applied. Namely, a pattern matching algorithm based on the minimum distance
133 from the previously identified centroids is used to assign each day and individual forecast member
134 to the closest weather regime (previously identified by using exclusively ERAI). The climatology
135 of the forecasted WRs is then calculated by summing the daily classification of each WR for all
136 the members and all the days inside a 30-day window. The same climatology is derived by using
137 ERAI. The Monthly Occurrence Anomaly of WRs (MOAWRs) is then calculated with respect to
138 the climatological occurrences based on the hindcast period (1992-2013) and obtained by using
139 independently both ERAI and ENS.

140 To potentially increase the signal emerging from the teleconnection between MOAWRs and
141 precipitation anomalies, different combinations (additions and subtractions of WR occurrences)
142 of two WRs are tested. This could be useful when two WRs have the same or opposite impacts
143 on precipitation. For example, in the case of two regimes WRa and WRb that are associated with,
144 respectively, dry and wet conditions over a certain region, the occurrence difference of the two
145 WRs could be more linked to the drought events over that region (this example will be discussed
146 later in the document). In total, a set of 6 to 12 combinations (see the list in Table 1) is tested when
147 3 or 4 WRs (depending the season) are detected, respectively.



148 *c. Drought metrics*

149 As suggested by the World Meteorological Organization, the Standardized Precipitation Index
150 (SPI) is one of the most relevant indicators providing a clear and robust characterization of pre-
151 cipitation deficiencies and it is a good proxy for assessing meteorological droughts. The SPI
152 calculation is relatively simple and it is performed independently at each grid point of the domain.
153 This method is robust and has the advantage of being flexible in time, for the accumulation period
154 studied, and in space, for the resolutions used. It also provides an unbiased product, which is
155 important for comparing datasets from observations and model simulations. In the SPI calcula-
156 tion, a gamma distribution is first fitted to precipitation data and then transformed into a standard
157 normal distribution (McKee et al. 1993, 1995; Svoboda et al. 2012). The choice of the statistical
158 distribution has been verified in Lavaysse et al. (2015) and shown that this assumption is valid
159 over a large proportion of Europe. Nevertheless, over the driest regions and in summer, some grid
160 points (mainly in Spain and South Italy) the significant tests are not verified. Both the observed
161 and modeled daily precipitation values are accumulated over a period of 30 days (i.e. we use the
162 SPI-1, where 1 refers to the accumulation period of one month). The choice of analyzing relatively
163 short meteorological droughts is based on two main constraints: i) a technical one connected to
164 the limitation of the extended ENS that provides forecasts up to 33 days in the version here an-
165 alyzed, and ii) the chaotic nature of the atmosphere that limits the predictability of precipitation
166 and geopotential forecasts after several weeks. This relative short term drought information is
167 also relevant for users and decision makers since it provides valuable information about the onset,
168 continuation or end of longer droughts.

169 Based on this approach, both observed and forecasted SPI-1 values are calculated for the pe-
170 riod 1992-2013. Here, a meteorological drought is defined as having SPI-1 values less than -1.



171 According to the normal distribution of the SPI, this threshold corresponds to about 17.5% of the
172 driest events. Based on Lavaysse et al. (2015), the most reliable method for producing a dichoto-
173 mous forecast of drought from probabilistic forecasts of precipitation, and more specifically from
174 the extended ENS of the ECMWF, is to predict a drought as soon as more than 30% of the ENS
175 members are associated with a drought forecast (i.e. $SPI-1 < -1$).

176 *d. Validation tools*

177 To assess the forecasts of drought events, traditional scores for dichotomous products are ap-
178 plied. These scores make use of the contingency table (Table 2) that shows the types of agreement
179 of observed and forecasted variables.

180 The percentage of observed events that had been correctly forecasted are provided by the
181 Probability Of Detection score (POD) whereas the percentage of events that had been forecasted
182 but did not occur are indicated by the False Alarm Rate (FAR). Finally, to take into account the
183 hits, misses and false alarms and to neglect the correct negative forecasts that will dump the
184 scores for rare events, the Gilbert Skill Score (GSS, Jolliffe and Stephenson 2003) is used. For
185 rare events, such as droughts, it is more relevant to use this score than the Peirce's skill score for
186 instance. The GSS indicates how well the forecasted droughts correspond to the observed ones.
187 This skill score is compared to the score obtained by the climatology. It is calculated as follows:

188

$$GSS = \frac{(hits - hits_c)}{(hits + misses + false\ alarms - hits_c)} \quad (1)$$

189 where $hits_c = \frac{(hits+misses)(hits+false\ alarms)}{total}$. Based on these equations, a perfect forecast achieves a
190 score equal to 1, while a score equal to 0 is assigned to the climatology (i.e. no forecast skill). All
191 these scores are calculated independently for each season.



192 **3. Configuration of the drought forecasts**

193 To forecast droughts using the MOAWRs approach, 3 steps are needed (see also Fig. 1 in the
194 supplementary material): 1) the WR classification (detailed previously and exclusively done with
195 ERAI); 2) the daily WR attribution, to determine which is the closest WR classified previously
196 for a forecasted (or reanalysis) geopotential anomaly for each day and member; 3) the predictor
197 assignment, to determine which WR is the best predictor of droughts for each grid point. This
198 last step is based on a best correlation criterion and leads to coherent picture (Fig. 1), highlighting
199 the large-scale impacts of the WRs. It is interesting to note that following this approach, the large
200 majority of SPI-1 in Europe is associated with a combination of WRs. The correlation values
201 used in the last step show significant spatial differences (Fig. 2). Throughout the year, they are
202 generally higher teleconnections in northern Europe than in southern Europe. This could explain
203 the larger variability of MOAWR predictors over Central than North Western Europe. There is
204 also a strong seasonal difference. In winter, the mean correlation is about 0.55 whereas it is about
205 0.28 in summer. The origin of precipitation, which is more synoptically-driven in winter and more
206 local in summer, can explain these results.

207 Once the attribution of WRs and the predictor assignment are done, the potential benefits is
208 assessed to analyze the limitations of using these predictors. To do so, 5 different drought fore-
209 casting approaches (that are differentiated by the methodologies employed for the three steps listed
210 previously) are used. The detailed configuration of these methodologies is provided in the supple-
211 mentary material, while a brief overview is here reported.



212 The first method of drought forecasting is based on forecasted precipitation (Lavaysse et al.
213 2015). The skill scores of this forecasting approach are here used as benchmark (see Table 6
214 for the list of these characteristics). The second approach, called 'idealized forecast', uses exclu-
215 sively the MOAWRs derived from ERAI and does not take into account the uncertainties related
216 to the forecasts of WRs. The third forecasting method, called operational forecast, is based on the
217 MOAWRs derived from the forecasted WRs of the ensemble model (nevertheless, ERAI is used
218 for the WR classification to avoid potential problem when the version of the operational model
219 changes). The fourth forecasting scheme, called optimized forecast, is similar to the previous one
220 but uses ENS for the WRs assignment. This methodology tends to optimize the forecasts by cor-
221 recting some bias in the forecasted MOAWRs. Finally the fifth forecasting method, called process
222 forecast, is similar to the others except for the use of modelled precipitation. This last approach
223 allows to analyze the modelled teleconnection between MOAWRs and SPI; therefore, it can be
224 used to investigate the skill of the model in representing observed processes.

225 4. Results

226 a. Skill scores

227 The skill scores of the forecasted precipitation, also called and presented in the previous section
228 as Reference and used as benchmark, provided by ENS and derived from Lavaysse et al. (2015),
229 where a drought is forecasted when at least 30% of members forecasts $SPI < -1$, are here shown.
230 The best achieved performance (for winter in Central Europe) shows how slightly more than 40%
231 of the observed drought events are correctly predicted with a 30-day lead time (Fig. 3a, d, g, j) with
232 about 60% of false alarms (Fig. 3b, e, h, k). For both POD and FAR, the spatial variability is small
233 (standard deviation lower than 0.2) especially during spring and fall. In winter, an improvement



234 can be noticed in Germany, Poland, Spain and Norway; whereas in summer, drought seems to be
235 more predictable in eastern Europe. When the POD and the FAR are combined in the integrated
236 GSS (Fig. 3c, f, i, l), higher seasonal and spatial differences appear. Overall, the score reaches
237 up to 0.3 in winter, especially in northern Germany [50deg.N, 10deg.E]; while the worst value
238 is reached in spring and summer, especially in western Europe (France, Belgium). Due to the
239 impacts of the local forcing on precipitation, the drought forecasts based on large-scale predictors
240 are better in continental than in coastal regions (more details in Lavaysse et al. (2015)).

241 The forecasts based on MOAWRs can now be assessed with respect to the precipitation-based
242 forecast (SPI-1). In order to detect the same number of drought events when using these predictors
243 and the precipitation, the threshold of the MOAWRs is chosen equal to 0.176 (0.824 for negative
244 correlations). The POD, FAR and GSS for the four seasons are shown in Fig. 4 using 20 years with
245 a leave-one-out technique, which is a cross-validation method for small samples sizes enabling to
246 validate results by simply partitioning the series into a training and a test part. To highlight the
247 benefits of this method, the anomaly with respect to the reference forecast (i.e. Fig. 3) are plotted.
248 The forecast based on MOAWRs is more spatially variable. As for winter in the northern part
249 of Europe, this forecast is significantly better in terms of both POD and GSS; whereas in central
250 Europe the forecast based on precipitation is more reliable. Despite the fact that the patterns are
251 less homogeneous for the other seasons, some positive impacts of this forecasting approach appear,
252 e.g. in: northern Russia in spring, western Europe in summer, central Europe during fall.

253 These results are consistent with the intensity of the teleconnection measured during the assign-
254 nation procedure between the SPI and the WRs (Fig. 2a) and highlight the regions where the
255 large-scale atmospheric patterns associated with the WRs could better explain strong precipitation
256 deficits when compared to local drivers (orography, soil moisture, coastline).



257 *b. Intensity and initial conditions*

258 To better understand the potential performance of the approach, sensitivity tests are conducted.
259 In the previous section, the SPI-1 intensity threshold to define a drought was fixed to -1. The
260 previously used skill scores are here derived for SPI lower than -1.5 and -2 (respectively $\sim 7\%$
261 and $\sim 2.5\%$ of the most extreme cases). A second sensitivity test is done on the initial conditions
262 influencing all results but also bringing useful information on drought onset and persistence. Most
263 of the studies on drought focuses on 3-month (or longer) cumulated precipitation that could have
264 more severe impacts on, e.g., agriculture and water resources. Due to the unpredictable nature
265 of the weather and the limitation of the lead time of the ENS model, the assessment of drought
266 forecasting is limited to 1-month lead time in our study. Nevertheless, the information of the two
267 previous months (observed SPI-2 with a threshold defined as -1) is taken into account to measure
268 the impacts of these initial conditions and the ability to forecast drought persistence/onset.

269 In Fig. 5 the GSS scores in winter for all the domain shown in the previous Figures are synthe-
270 sized by using boxplots. The results shown in Fig. 3a and Fig. 4a are represented by the black
271 boxplots plotted for $\text{SPI} < -1$ in Fig. 5a and b respectively. Overall, the predictability decreases
272 with the drought intensity. In winter, dry initial conditions generate a favorable environment to
273 better forecast droughts. In other words, the persistence of drought is better predicted than the
274 onset. Finally, the last main result concerns the improvement of the forecasts based on MOAWRs.
275 For the SPI lower than -1, all GSS values shown in Fig. 5 are quite close. But, as also highlighted
276 by Fig. 4, there is a larger spatial variability with the MOAWRs approach. For more intense
277 droughts, there is a global and significant improvement with MOAWRs. Indeed for drought in-
278 tensities with SPI lower than -2, the median of the GSS scores goes up from close to 0 (using the



279 precipitation-based method) to 0.05 (using the MOAWRs). This result is mainly explained by the
280 better predictability of the drought onset (right blue boxes in Fig. 5a and b).

281 The same sensitivity tests are conducted for the others seasons (not shown), and the decrease
282 of predictability with increasing drought intensity is found for all of them. Nevertheless, the
283 conclusions on the role of the initial conditions depend on the season. For instance in summer,
284 drought onsets are slightly better predicted than drought persistence. The reason could be the
285 higher temporal variability of the monthly precipitation deficits in summer than in winter due to
286 the larger impact of local forcings. Finally in all the seasons, the use of atmospheric predictors
287 leads to better performance when looking at the most extreme events ($SPI < -2$).

288 **5. Sources of uncertainty**

289 To better discuss and understand the previous results and their uncertainties, additional tests
290 are here reported. The main objective is to quantify the contribution of the uncertainties in WR
291 predictions and the teleconnection between the SPI and the WRs.

292 *a. Validation of the WR forecasts*

293 The first question to address is about the quality of the forecasts of MOAWRs. The method
294 used is based on the total occurrence of each WR among all the members and the entire lead time
295 (5 members* 30-day LT). The anomalies are then calculated in relation to the climatology of the
296 forecasts. These anomalies are divided by the number of ensemble members to create comparable
297 results with the data provided by ERAI.

298 To validate the forecast of the WRs, first the comparison of the frequency of occurrence of each
299 daily WR is performed (Fig. 6). The WR-distributions as given by the forecasts are characterized
300 by a higher degree of similarity than the ones given by ERAI, with a peak of occurrence at around



301 5-8 days in winter (blue bars, Fig. 6). The same holds for the other seasons (not shown). The lower
302 spread of the forecasted WR occurrences, associated with reduced tails (i.e. reduced occurrences
303 for durations exceeding 20 days), could be explained by the underestimation of the long-term
304 blocking. A further examination of the temporal evolution of these occurrence anomalies suggests
305 that the distribution of forecasted drought occurrences (previously shown) could mainly explain
306 the overestimation of low occurrences in the observations (i.e., larger number of forecasted events
307 compared to observed ones with durations shorter than 5 days) and the underestimation of longer
308 duration events (i.e., lower forecasted than observed events with durations longer than 15 days, red
309 dotted lines in Fig. 7). Despite this behavior, the correlations appear significant with a maximum
310 of 0.65 for the WRa (significance with 90% of confidence at 0.58). These significant scores are
311 obtained in winter, while for the other seasons the correlations are lower (see Table 6). In summer,
312 they are not significant for two-thirds of the WRs.

313 *b. Strength of MOAWR-precipitation teleconnection*

314 According to the previous subsection, the WR forecast could be improved. Thus, it is important
315 to assess the limitation of the method using predictors and so assessing the strength of the MOAWR
316 and precipitation teleconnection. To this aim, the procedure 'idealized forecasts' of MOAWRs, e.g.
317 provided by ERAI without uncertainties on forecast, are compared to the forecast of precipitation
318 discussed and shown in Fig. 3.

319 The POD scores are strongly improved between seasons and regions (Fig. 8a, d, g, and j). These
320 results are strongly connected to the correlation values obtained and shown in Fig. 2 with the same
321 North-South and seasonal variabilities being observed. However, almost all the grid points show
322 a better POD with the WR predictors than with the precipitation-based forecasts. Up to 70% of
323 observed drought events are correctly detected in northern Europe during winter. This percentage



324 falls to about 17.5% in summer (i.e., the climatological value) in the southern part of the domain.
325 The results in terms of FAR are more variable depending on both the season and the region. On
326 average, there is a small decrease of the FAR. However, the GSS shows a clear and significant
327 improvement in the drought forecast when using the WR predictors. Compared to the scores using
328 real forecasts in Fig. 4, the bigger difference is more in terms of intensities than in the spatial
329 distribution. For instance, in winter a high improvement is observed in northern Europe (up to 0.2
330 against 0.1 for the real forecast over Scandinavia) whereas a decrease/close score is obtained in
331 central Europe. Based on this sensitive analysis, the teleconnection between the SPI-1 < -1 and the
332 MOAWRs is strong enough to provide significant improvements of the prediction scores in most
333 of the regions. Nevertheless, this analysis also highlights the limitations of the methods used in
334 this study when and where the influence of the WR on drought is lower (i.e. Germany and Poland
335 in winter; eastern Europe in summer; southern Europe in fall).

336 *c. Modeled teleconnection*

337 Some additional tests are also conducted on the predictor assignation procedures (definition of
338 the best predictant for SPI-1 < -1 at each grid point) to see the impacts of using either ERAI
339 or ENS (the latter could potentially correct bias of the ENS, see the supplementary material for
340 more details). Due to the errors associated with the WR forecasts, the procedures using WRs
341 from ERAI or ENS provide different results (Fig. 9a, c compared to Fig. 1). The assignation pat-
342 terns done with the WRs provided by ERAI (Fig. 1) have less homogeneous large-scale structures
343 (i.e., more spatial variability) than those provided by the WRs forecasted by ENS (Fig. 9a and c)
344 showing a more complex observed than forecasted teleconnections. Nevertheless over continental
345 regions, there are some similarities between the assigned predictors obtained by using ENS and
346 ERAI (impact of WRs b, b-a, a, c-d), illustrating the relative good representation of the impacts



347 of specific WR on precipitation by ENS. The correlation between the WRs forecasted and the
348 observed precipitation are then plotted (Fig. 9b). The correlation values, which can be compared
349 to the correlation shown in Fig. 2a, are quite low as a result of the relatively low predictability of
350 the WRs previously discussed and where the teleconnection between WRs and precipitation is the
351 highest (i.e. in southern Norway and the northern part of the U.K.).

352 The last analysis is focused on the modeled teleconnection between the SPI and the WRs both
353 provided by the ENS (Fig. 9c and 9d). It is remarkable the great similarities of the maps for the
354 assignments and the observed teleconnection by using observations and reanalysis (correlation
355 values greater than 0.65, Fig. 1 and 2a). This is especially true over the U.K, Ireland, Scandinavia,
356 Spain and north-western Russia. Some differences are observed in southern France and Italy where
357 the model overestimates the large-scale forcing on precipitation (i.e. with stronger correlation with
358 WRs than observed). This highlights the overall good representation of the processes linking large
359 scale circulation and precipitation deficits by ENS. So the ENS model succeeds in capturing the
360 impacts of the WR occurrence on the precipitation anomalies as shown in the observations over a
361 large part of Europe. These results could suggest limitations in using such predictors as the lack of
362 skill score could result from a failure in forecasting the large-scale atmospheric circulation (rather
363 than from a misrepresentation of the physical processes).

364 **6. Conclusion**

365 In this study, a drought forecasting method based on large-scale atmospheric predictors is pro-
366 posed in order to improve the early warning of atmospheric drought events. The method is based
367 on the Monthly Occurrence Anomalies of Weather Regimes (MOAWRs) within a 30-day lead-
368 time. The methodology used to select the predictors is based on a three step procedure. First, WRs
369 (described by daily geopotential anomalies) are identified by using a Genetic K-means algorithm



370 for each season separately and for both ERAI and extended ENS forecasts. The climatological
371 occurrences are calculated for each WR. The identified three/four WRs (depending on the sea-
372 son) are combined (added or subtracted) with each other to enhance the potential signal of their
373 impacts. Second, the MOAWRs is used as a predictor of meteorological droughts at each grid
374 point. The predictor assignation procedure is based on the correlation between the MOAWRs and
375 the SPI-1. To select the best predictor, the MOAWR associated with the strongest absolute value
376 of correlation is selected. The last step involves the forecasting of the SPI-1 lower than -1. Two
377 approaches are derived and compared. The first one is based on the index developed by Lavaysse
378 et al. (2015) for drought events and derived from the forecasted precipitation provided by the ENS.
379 This represents a benchmark for the early warning of drought forecasting. At most around 40% of
380 drought events are detected one month in advance with 65% of false alarms. The second forecast-
381 ing approach is based on MOAWRs. In the northern and eastern parts of the European continent,
382 an improvement of the Gilbert Skill Score (GSS) is observed w.r.t. the precipitation-based one.
383 Nevertheless, this is balanced by other regions where the forecast skills is clearly lower (central
384 Europe in winter, eastern Europe in summer) than a precipitation based one. The origin of this
385 spatial and temporal variability in the skill scores is associated with the dynamic of precipitation.
386 In winter, precipitation is much more related to large-scale atmospheric forcing mainly captured
387 by the MOAWRs. On the contrary in summer, precipitation is more affected by local forcings
388 that could influence, for instance, the trajectory and the occurrence of convective systems. In this
389 study, this behavior is captured by the better correlation between MOAWRs and precipitation in
390 winter than in summer. The spatially variable skill scores is mainly controlled by the intensity
391 of the teleconnection between the MOAWRs and SPI-1. Due to the location of the geopotential
392 anomalies and the induced wind fields, or connected with the local effects that reduce the influ-
393 ence of the large scale forcing, the impacts of these MOAWRs on precipitation could be low, as



394 observed in winter over central Europe. According to these scores, the most reliable forecast could
395 result from choosing the best method for each grid point independently. The influence of the initial
396 conditions and the intensity of the drought highlight i) the losses of predictability with increasing
397 drought intensity and ii) the better scores in predicting persistency rather than the onset of drought
398 especially in winter. Also, the benefits of using the WRs to predict droughts appear to be more
399 important when the most intense droughts (i.e. $SPI < -2$) are forecasted.

400 This study shows the importance of improving the prediction of the WR occurrences. The
401 methodology applied here could be compared to more complex methodologies using clustering of
402 the members to define the most probable scenario, or by taking into account the transition between
403 WRs. Future work should also take into account the uncertainties in WR prediction. Recent
404 studies (Matsueda and Palmer 2014, 2015) have shown that WR prediction is still a big challenge
405 with regard to lead-times greater than 15 days. Some improvements could be also done by using
406 a multi-model ensemble such as the one recently developed in the framework of the Seasonal to
407 Sub-Seasonal (S2S) project (Vitart et al. 2016).

408 *Acknowledgments.*

409 **References**

- 410 Boé, J., 2013: Modulation of soil moisture–precipitation interactions over France by large scale
411 circulation. *Climate dynamics*, **40** (3-4), 875–892.
- 412 Cassou, C., L. Terray, and A. S. Phillips, 2005: Tropical atlantic influence on european heat waves.
413 *Journal of climate*, **18** (15), 2805–2811.
- 414 Cattiaux, J., R. Vautard, C. Cassou, P. Yiou, V. Masson-Delmotte, and F. Codron, 2010: Winter
415 2010 in Europe: a cold extreme in a warming climate. *Geophysical Research Letters*, **37** (20).



- 416 Dee, D., and Coauthors, 2011: The ERA-Interim reanalysis: Configuration and performance of
417 the data assimilation system. *Quarterly Journal of the Royal Meteorological Society*, **137 (656)**,
418 553–597.
- 419 Ferranti, L., S. Corti, and M. Janousek, 2015: Flow-dependent verification of the ecmwf ensemble
420 over the euro-atlantic sector. *Quarterly Journal of the Royal Meteorological Society*, **141 (688)**,
421 916–924.
- 422 Guérémy, J.-F., N. Laanaia, and J.-P. Céron, 2012: Seasonal forecast of French Mediterranean
423 heavy precipitating events linked to weather regimes. *Natural Hazards and Earth System Sci-*
424 *ence*, **12 (7)**, 2389–2398.
- 425 Haiden, T., M. Janousek, J. Bidlot, L. Ferranti, F. Prates, F. Vitart, P. Bauer, and D. Richardson,
426 2017: Evaluation of ECMWF forecasts, including 2016-2017 upgrades. *ECMWF - Technical*
427 *Memorandum*, **(817)**.
- 428 Häkkinen, S., P. B. Rhines, and D. L. Worthen, 2011: Atmospheric blocking and atlantic multi-
429 decadal ocean variability. *Science*, **334 (6056)**, 655–659.
- 430 Haylock, M., N. Hofstra, A. Klein Tank, E. Klok, P. Jones, and M. New, 2008: A European
431 daily high-resolution gridded data set of surface temperature and precipitation for 1950–2006.
432 *Journal of Geophysical Research: Atmospheres (1984–2012)*, **113 (D20)**.
- 433 Hurrell, J. W., Y. Kushnir, G. Ottersen, and M. Visbeck, 2003: *An overview of the North Atlantic*
434 *Oscillation*. Wiley Online Library.
- 435 Jolliffe, I., and D. Stephenson, 2003: Forecast verification: A practitioners guide in atmospheric
436 science.



- 437 Kingston, D. G., J. H. Stagge, L. M. Tallaksen, and D. M. Hannah, 2015: European-scale drought:
438 understanding connections between atmospheric circulation and meteorological drought in-
439 dices. *Journal of Climate*, **28** (2), 505–516.
- 440 Lavaysse, C., J. Vogt, and F. Pappenberger, 2015: Early warning of drought in Europe using the
441 monthly ensemble system from ECMWF. *Hydrology and Earth System Sciences Discussions*,
442 **12** (2), 1973–2009.
- 443 Matsueda, M., and T. Palmer, 2014: Predictability of wintertime Euro-Atlantic weather regimes
444 in medium-range forecasts. *EGU General Assembly Conference Abstracts*, Vol. 16, 12945.
- 445 Matsueda, M., and T. Palmer, 2015: Predictability of summertime Euro-Atlantic weather regimes
446 in medium-range forecasts. *EGU General Assembly Conference Abstracts*, Vol. 17, 11809.
- 447 McKee, T. B., N. J. Doesken, and J. Kleist, 1995: Drought monitoring with multiple time scales.
448 *Proceedings of the 9th Conference on Applied Climatology*, American Meteorological Society
449 Dallas, Boston, MA, 233–236.
- 450 McKee, T. B., N. J. Doesken, J. Kleist, and Coauthors, 1993: The relationship of drought fre-
451 quency and duration to time scales. *Proceedings of the 8th Conference on Applied Climatology*,
452 American Meteorological Society Boston, MA, USA, Vol. 17, 179–183.
- 453 Michelangeli, P.-A., R. Vautard, and B. Legras, 1995: Weather regimes: Recurrence and quasi
454 stationarity. *Journal of the Atmospheric Sciences*, **52** (8), 1237–1256.
- 455 Molteni, F., R. Buizza, T. N. Palmer, and T. Petroliagis, 1996: The ECMWF ensemble prediction
456 system: Methodology and validation. *Quarterly Journal of the Royal Meteorological Society*,
457 **122** (529), 73–119.



- 458 Peings, Y., and G. Magnusdottir, 2014: Forcing of the wintertime atmospheric circulation by the
459 multidecadal fluctuations of the north atlantic ocean. *Environmental Research Letters*, **9** (3),
460 034 018.
- 461 Pfahl, S., 2014: Characterising the relationship between weather extremes in Europe and synoptic
462 circulation features. *Natural Hazards and Earth System Science*, **14** (6), 1461–1475.
- 463 Plaut, G., and E. Simonnet, 2001: Large-scale circulation classification, weather regimes, and
464 local climate over France, the Alps and western Europe. *Climate Research*, **17** (3), 303–324.
- 465 Robertson, A. W., and M. Ghil, 1999: Large-scale weather regimes and local climate over the
466 western United States. *Journal of Climate*, **12** (6), 1796–1813.
- 467 Santos, J., J. Corte-Real, and S. Leite, 2005: Weather regimes and their connection to the winter
468 rainfall in Portugal. *International Journal of Climatology*, **25** (1), 33–50.
- 469 Stephenson, D., A. Hannachi, and A. O’Neill, 2004: On the existence of multiple climate regimes.
470 *Quarterly Journal of the Royal Meteorological Society*, **130** (597), 583–605.
- 471 Svoboda, M., M. Hayes, , and D. Hood, 2012: Standardized precipitation index user guide. *World*
472 *Meteorological Organization*, Report WMO–No. 1090, Geneva.
- 473 Toreti, A., E. Xoplaki, D. Maraun, F. Kuglitsch, H. Wanner, J. Luterbacher, and Coauthors, 2010:
474 Characterisation of extreme winter precipitation in Mediterranean coastal sites and associated
475 anomalous atmospheric circulation patterns. *Nat. Hazards Earth Syst. Sci.*, **10** (5), 1037–1050.
- 476 Vitart, F., 2014: Evolution of ECMWF sub-seasonal forecast skill scores. *Quarterly Journal of the*
477 *Royal Meteorological Society*, **140** (683), 1889–1899.
- 478 Vitart, F., and Coauthors, 2016: The sub-seasonal to seasonal prediction (s2s) project database.
479 *Bulletin of the American Meteorological Society*, (2016).



- 480 Wanner, H., S. Brönnimann, C. Casty, D. Gyalistras, J. Luterbacher, C. Schmutz, D. B. Stephen-
481 son, and E. Xoplaki, 2001: North Atlantic Oscillation—concepts and studies. *Surveys in geo-*
482 *physics*, **22** (4), 321–381.
- 483 Yiou, P., and J. Cattiaux, 2013: Contribution of atmospheric circulation to wet north European
484 summer precipitation of 2012. *Bulletin of the American Meteorological Society*, **94** (9), S39.
- 485 Yiou, P., and M. Nogaj, 2004: Extreme climatic events and weather regimes over the North At-
486 lantic: When and where? *Geophysical Research Letters*, **31** (7).
- 487 Zampieri, M., A. Toreti, A. Schindler, E. Scoccimarro, and S. Gualdi, 2017: Atlantic multi-decadal
488 oscillation influence on weather regimes over europe and the mediterranean in spring and sum-
489 mer. *Global and Planetary Change*, **151**, 92–100.



490 **LIST OF TABLES**

491	Table 1.	Definition of the four sets of forecasts compared in that study. The differences	
492		are based on the use of predictor or not, the use of reanalysed or forecasted	
493		WRs as predictor and for the assignation procedure and on the use of observed	
494		or forecasted SPI during the assignation procedure.	25
495	Table 2.	Definition of WRs and WR combinations. * indicate regimes that exist only in	
496		winter and spring.	26
497	Table 3.	Contingency table of dichotomous events illustrating the four types of classifi-	
498		cation between observed and forecasted events.	27
499	Table 4.	Correlation values between the WR occurrence forecasted and observed for	
500		each WRs and the four seasons. Values indicated in bold have a significance	
501		level above 0.9.	28



Name	MOAWR predictor	WR for assignation	SPI for assignation
Reference	no predictor (Precip. forecast)	-	-
Idealized	ERA-Interim (ERA-Interim)	ERA-Interim	Observed
Operational	ENS	ERA-Interim	Observed
Optimized	ENS	ENS	Observed
Process	ENS	ENS	Forecasted (ENS)

502 TABLE 1. Definition of the four sets of forecasts compared in that study. The differences are based on the use
503 of predictor or not, the use of reanalysed or forecasted WRs as predictor and for the assignation procedure and
504 on the use of observed or forecasted SPI during the assignation procedure.



WR	A	B	C	D
A	WRa (#13)	a+b (#07)	a+c (#08)	a+d (#09)*
B	a-b (#01)	WRb (#14)	b+c (#10)	b+d (#11)*
C	a-c (#02)	b-c (#04)	WRc (#15)	c+d (#12)*
D	a-d (#03)*	b-d (#05)*	c-d (#06)*	WRd (#16)*

TABLE 2. Definition of WRs and WR combinations. * indicate regimes that exist only in winter and spring.



		Event observed	
		Yes	No
Event	Yes	hits	false alarms
Forecasted	No	misses	correct negative

505 TABLE 3. Contingency table of dichotomous events illustrating the four types of classification between ob-
506 served and forecasted events.



Season	WR	Correlation	Season	WR	Correlation
Winter	A	0.65	Spring	A	0.48
	B	0.52		B	0.43
	C	0.57		C	0.47
	D	0.57		D	0.62
Summer	A	0.45	Autumn	A	0.51
	B	0.42		B	0.47
	C	0.47		C	0.47

507 TABLE 4. Correlation values between the WR occurrence forecasted and observed for each WRs and the four
508 seasons. Values indicated in bold have a significance level above 0.9.



509 **LIST OF FIGURES**

510 **Fig. 1.** Automatic attribution of the best predictors in winter based on the occurrence anomalies of
 511 WRs of ERAI and the observed precipitation. The names of the predictors are indicated in
 512 the color scale. 30

513 **Fig. 2.** Absolute values of temporal correlation between SPI-1 and MOAWR attributed from the
 514 16 combinations in winter (a), spring (b), summer (c) and autumn (d). Only values with a
 515 confidence level larger than 90% are plotted. 31

516 **Fig. 3.** POD (left panels), FAR (centre panels) and GSS (right panels) scores of droughts prediction
 517 calculated using the forecasted precipitation. The scores are calculated for (from top to
 518 bottom) winter (first), spring (second), summer (third) and autumn (fourth line). 32

519 **Fig. 4.** Anomalies of POD (left panels), FAR (centre panels) and GSS*2 (right panels) scores of
 520 drought prediction calculated using the MOAWR in relation to the forecasted precipitation
 521 (see Fig. 7). The scores are calculated for (from top to bottom) winter (first), spring (second),
 522 summer (third) and autumn (fourth line). Improvement scores by using the predictors are
 523 indicated in green (inverse scale for FAR). Only difference with confidence interval larger
 524 than 90% are plotted. 33

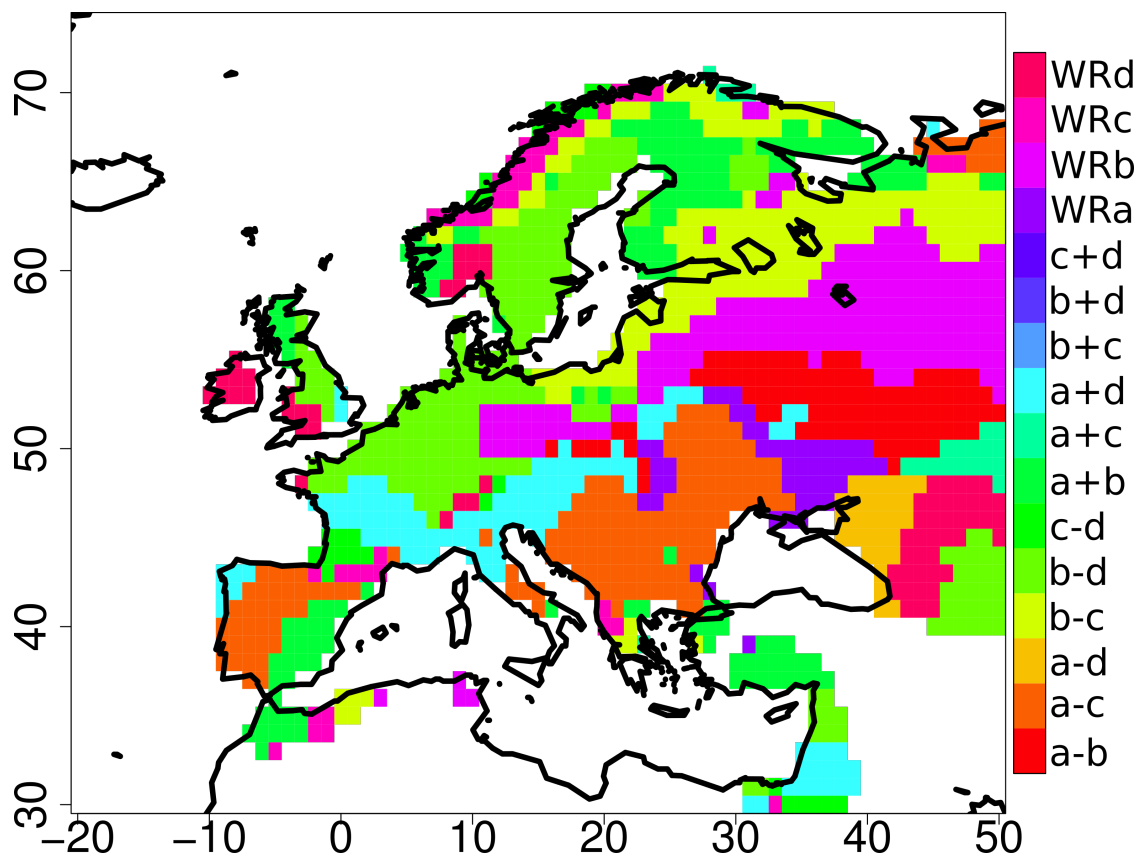
525 **Fig. 5.** Boxplot of the GSS scores in winter using the forecasted precipitation (a) and the MOAWRs
 526 (b). The scores are calculated over the entire domain and the boxes display the spatial
 527 variability. The scores are depending to the SPI intensities (-1, -1.5 and -2, x-axis) and
 528 the initial conditions defined by the previous SPI-2 conditions (see text for more details).
 529 Crosses indicate the scores but calculated by merging all the grid cells. 34

530 **Fig. 6.** Example of frequency distribution of WR occurrences (in days per 30-day windows) in
 531 winter for WR-A (a), WR-B (b), WR-C (c) and WR-D (d) using ERAI and ENS (red and
 532 blue bars respectively, purple when the two overlap). 35

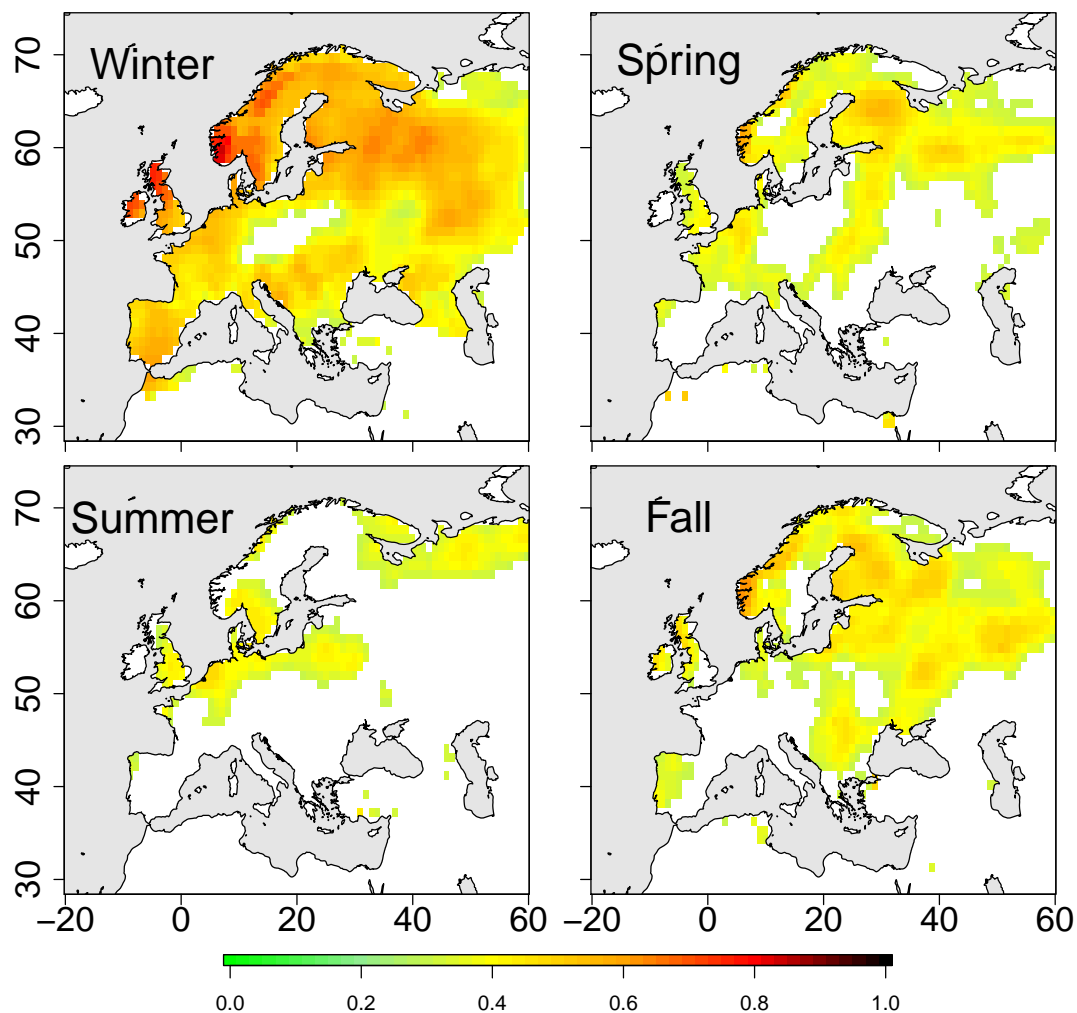
533 **Fig. 7.** Scatter plots of the occurrence of the four winter WRs provided by ERAI (x axis) and pro-
 534 vided by ENS (y axis). The linear least square regression are indicated with red dashed lines
 535 and the correspondent correlation on the top right of each panel. 36

536 **Fig. 8.** Anomalies of POD (left panels), FAR (middle panels) and GSS*2:w (right panels) of the
 537 drought prediction based on idealized forecasts of drought (using ERAI) and on precip-
 538 itation forecasts, in winter (first), spring (second), summer (third) and fall (fourth line).
 539 Improvement scores by using the predictors are indicated in green (inverse scale for FAR).
 540 Only difference with confidence interval larger than 90% are plotted. 37

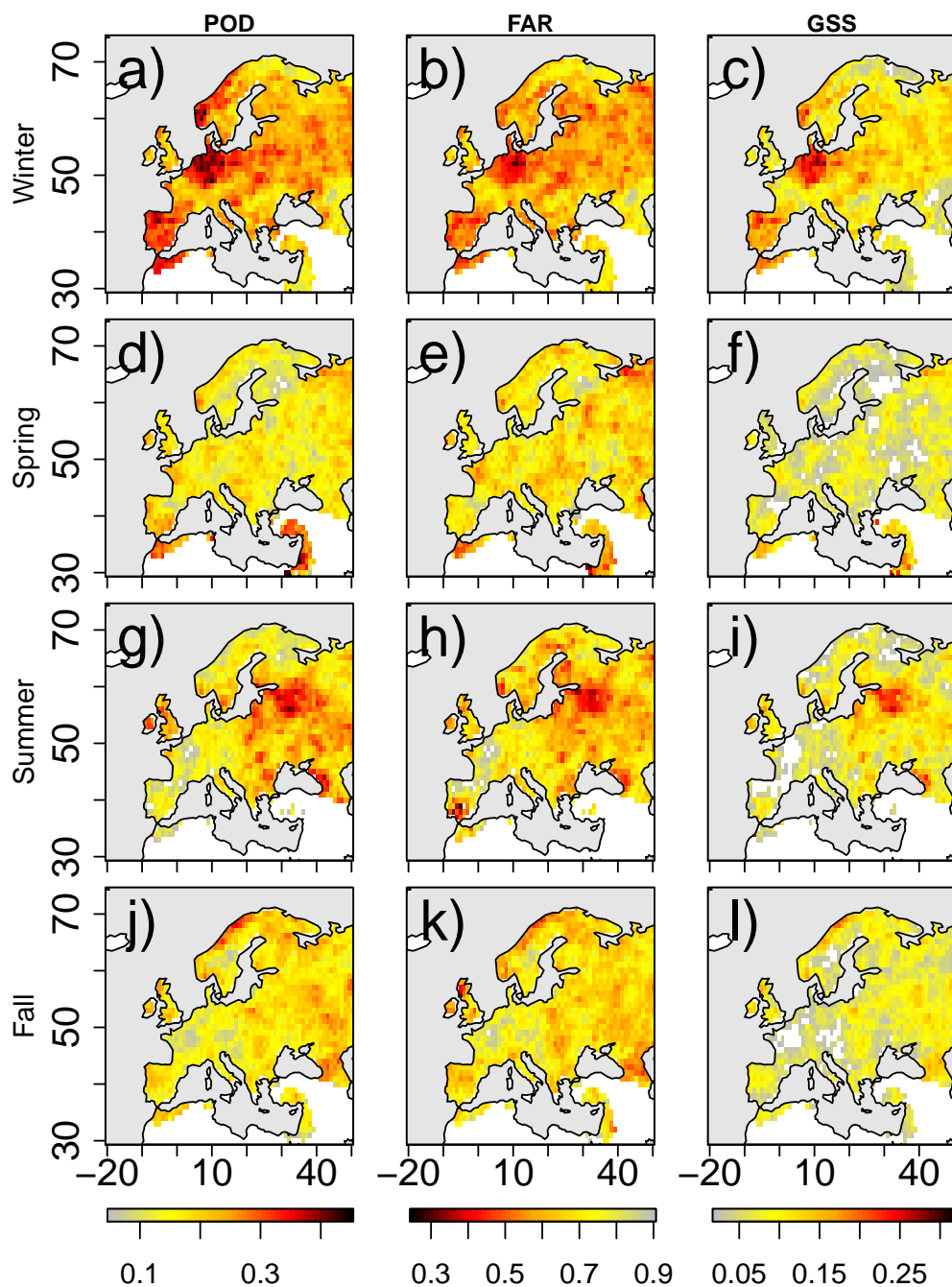
541 **Fig. 9.** Assigned winter WR (left panels) and associated correlation values (right panels) for 'Op-
 542 timized Forecast' (top): predictors defined using MOAWRs from ENS and observed SPI-1
 543 (a), correlation calculated between the forecasted MOAWRs and observed SPI-1 (b); and
 544 'Process Forecast' (bottom): predictors defined using MOAWRs from ENS and forecasted
 545 SPI-1 (c), correlation calculated between the forecasted MOAWRs and the forecasted SPI-1
 546 (d). 38



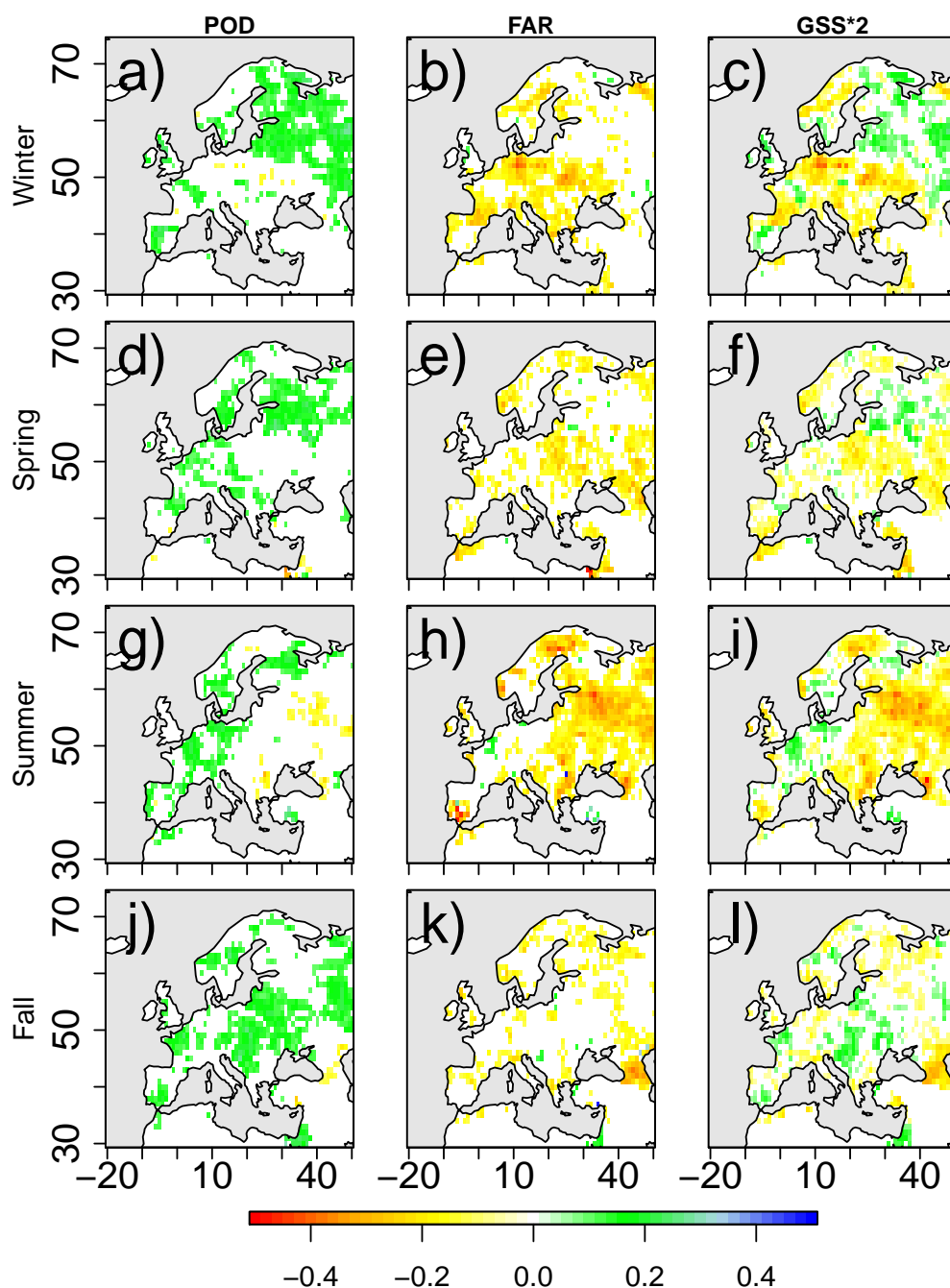
547 FIG. 1. Automatic attribution of the best predictors in winter based on the occurrence anomalies of WRs of
548 ERAI and the observed precipitation. The names of the predictors are indicated in the color scale.



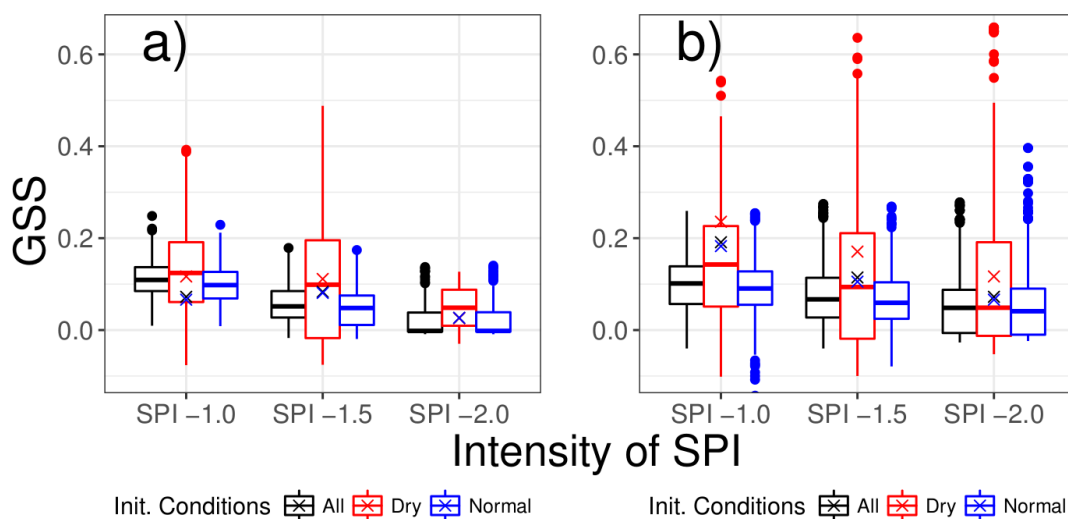
549 FIG. 2. Absolute values of temporal correlation between SPI-1 and MOAWR attributed from the 16 combina-
550 tions in winter (a), spring (b), summer (c) and autumn (d). Only values with a confidence level larger than 90%
551 are plotted.



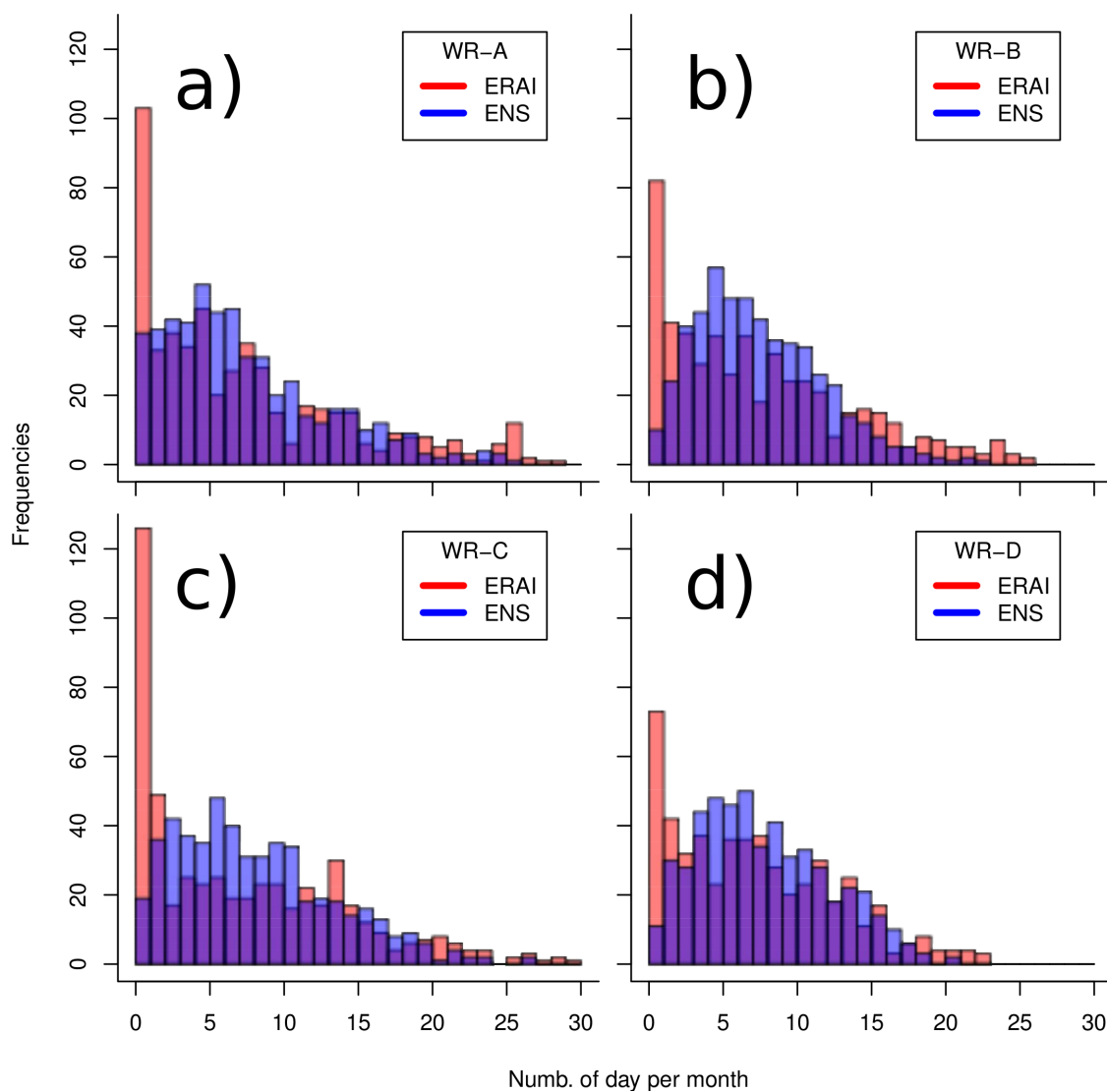
552 FIG. 3. POD (left panels), FAR (centre panels) and GSS (right panels) scores of droughts prediction calculated
553 using the forecasted precipitation. The scores are calculated for (from top to bottom) winter (first), spring
554 (second), summer (third) and autumn (fourth line).



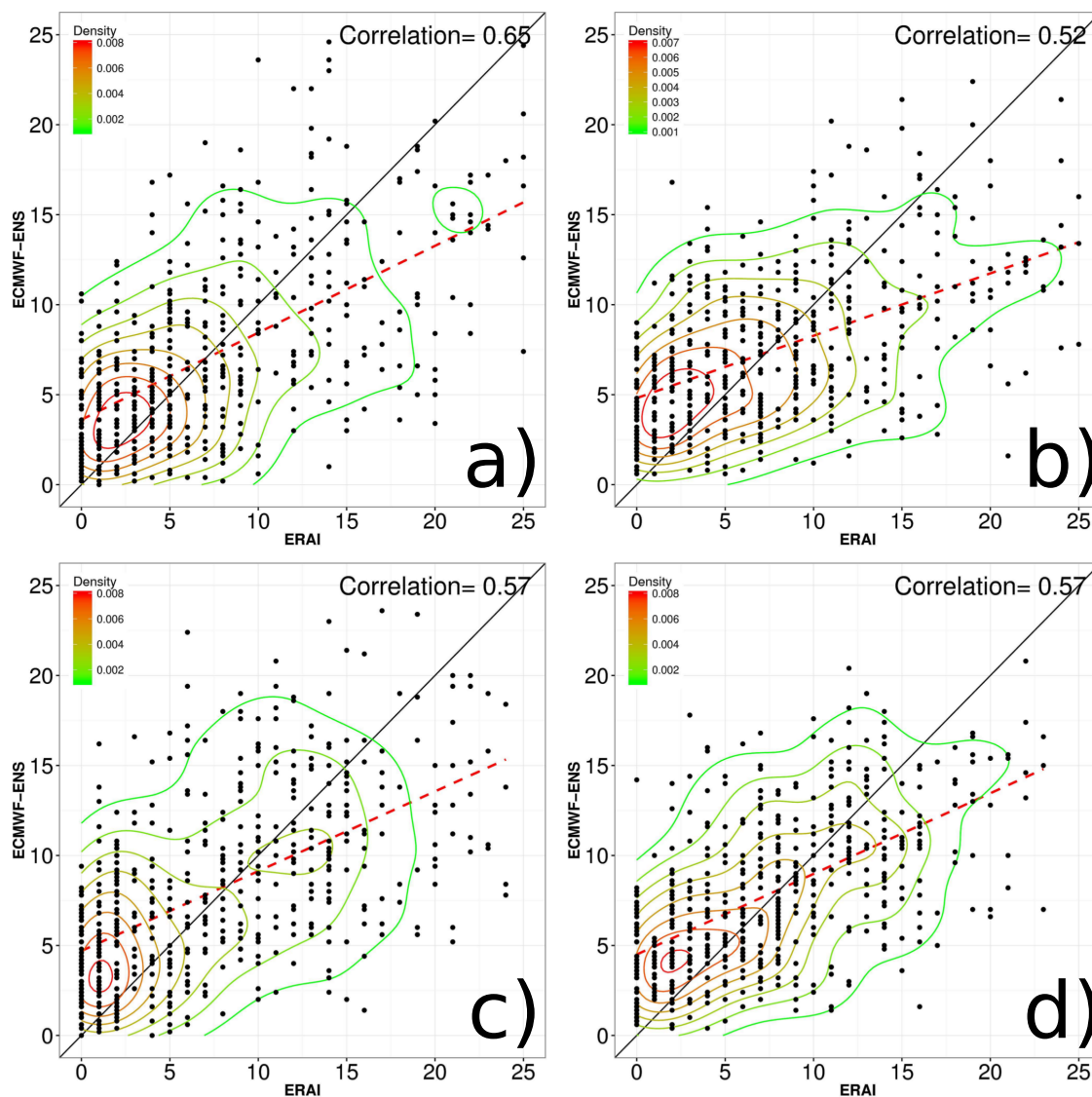
555 FIG. 4. Anomalies of POD (left panels), FAR (centre panels) and GSS*2 (right panels) scores of drought
 556 prediction calculated using the MOAWR in relation to the forecasted precipitation (see Fig. 7). The scores
 557 are calculated for (from top to bottom) winter (first), spring (second), summer (third) and autumn (fourth line).
 558 Improvement scores by using the predictors are indicated in green (inverse scale for FAR). Only difference with
 559 confidence interval larger than 90% are plotted.



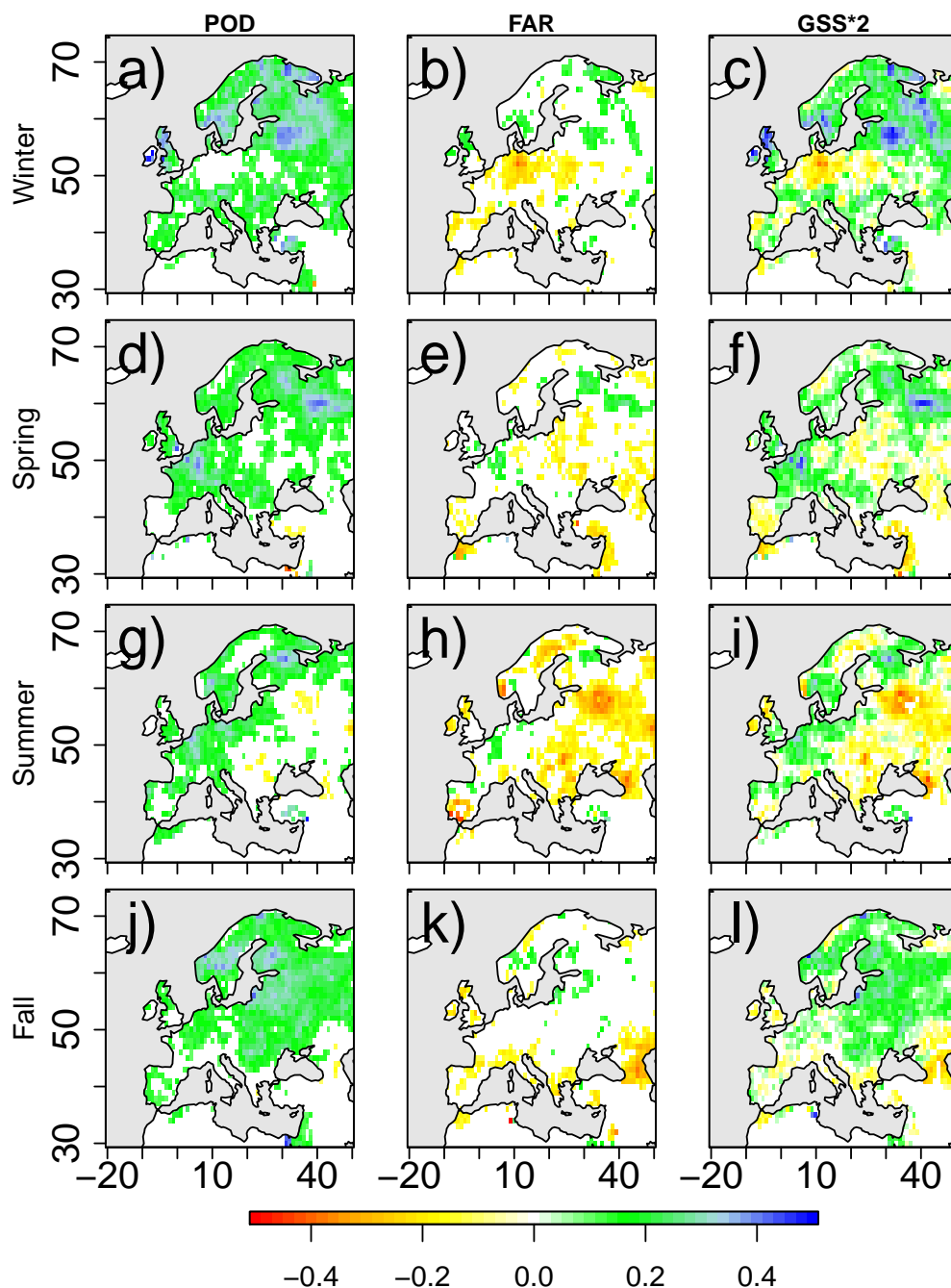
560 FIG. 5. Boxplot of the GSS scores in winter using the forecasted precipitation (a) and the MOAWRs (b).
561 The scores are calculated over the entire domain and the boxes display the spatial variability. The scores are
562 depending to the SPI intensities (-1, -1.5 and -2, x-axis) and the initial conditions defined by the previous SPI-2
563 conditions (see text for more details). Crosses indicate the scores but calculated by merging all the grid cells.



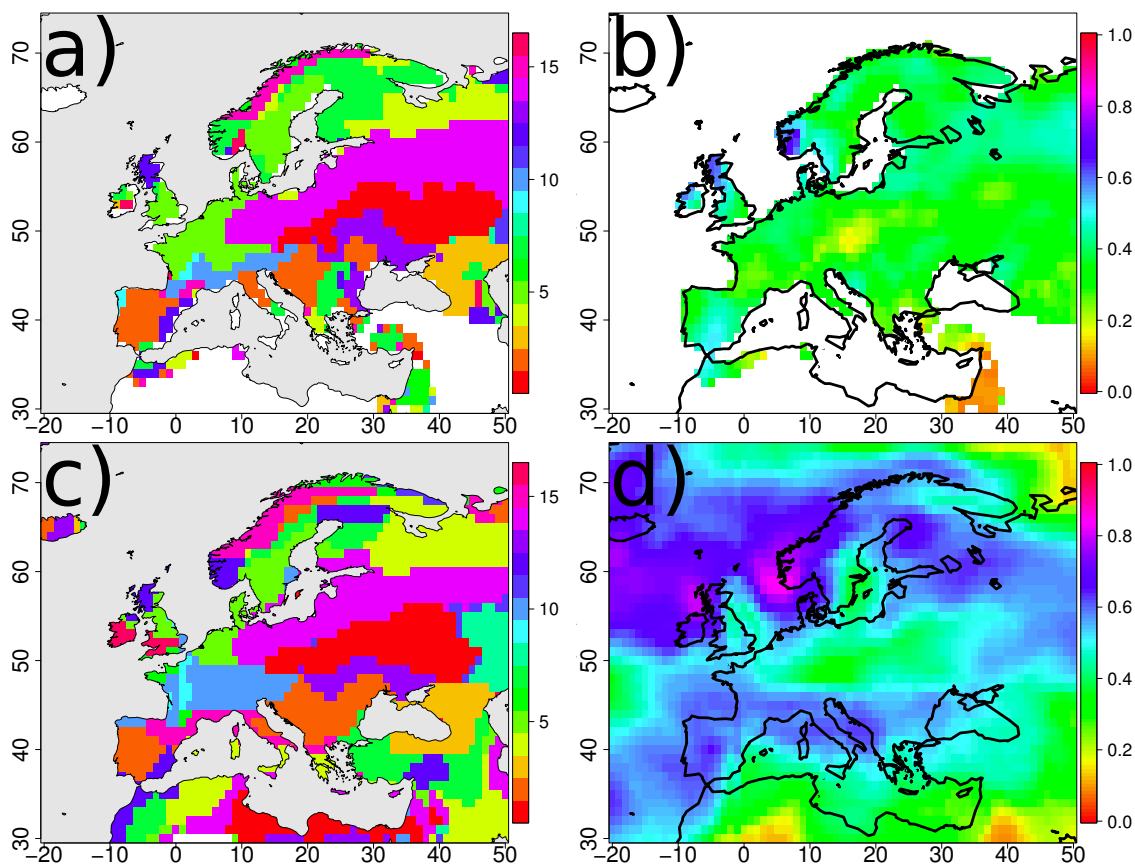
564 FIG. 6. Example of frequency distribution of WR occurrences (in days per 30-day windows) in winter for
565 WR-A (a), WR-B (b), WR-C (c) and WR-D (d) using ERAI and ENS (red and blue bars respectively, purple
566 when the two overlap).



567 FIG. 7. Scatter plots of the occurrence of the four winter WRs provided by ERAI (x axis) and provided
568 by ENS (y axis). The linear least square regression are indicated with red dashed lines and the correspondent
569 correlation on the top right of each panel.



570 FIG. 8. Anomalies of POD (left panels), FAR (middle panels) and GSS*2:w (right panels) of the drought
 571 prediction based on idealized forecasts of drought (using ERAI) and on precipitation forecasts, in winter (first),
 572 spring (second), summer (third) and fall (fourth line). Improvement scores by using the predictors are indicated
 573 in green (inverse scale for FAR). Only difference with confidence interval larger than 90% are plotted.



574 FIG. 9. Assigned winter WR (left panels) and associated correlation values (right panels) for 'Optimized
575 Forecast' (top): predictors defined using MOAWRs from ENS and observed SPI-1 (a), correlation calculated
576 between the forecasted MOAWRs and observed SPI-1 (b); and 'Process Forecast' (bottom): predictors defined
577 using MOAWRs from ENS and forecasted SPI-1 (c), correlation calculated between the forecasted MOAWRs
578 and the forecasted SPI-1 (d).